Available online at www.sciencedirect.com
ScienceDirect
Earth and Planetary Science Letters 252 (2006) 72–81
EPSL
www.elsevier.com/locate/epsl

Late Pliocene monsoon linkage in the tropical South China Sea

Jun Tian [a,b,*], Dorothy K. Pak [c], Pinxian Wang [a], David Lea [c], Xinrong Cheng [a], Quanhong Zhao [a]

[a] State Key Laboratory of Marine Geology, Tongji University, Shanghai 200092, PR China
[b] Department of Geosciences and Research Centre Ocean Margins (RCOM), Bremen University, D-28359 Bremen, Germany
[c] Department of Geological Sciences and Marine Science Institute, University of California, Santa Barbara CA 93106, USA

Received 19 May 2006; received in revised form 10 September 2006; accepted 11 September 2006
Available online 20 October 2006
Editor: M.L. Delaney

Abstract

The onset of Northern Hemisphere Glaciation (NHG) ~2.7 Ma ago coincided with prominent climate changes in the tropical regions such as the African and the Asian monsoons. However, the relationship between tropical and sub-tropical monsoonal variations and high northern latitude ice sheet expansion as well as processes such as late Pliocene tropical sea surface temperature (SST) change is not clear. Our late Pliocene (2.5–3.3 Ma) monsoon proxy records and Mg/Ca derived SST records at Ocean Drilling Program (ODP) Site 1143 from the southern South China Sea (SCS) reveal that while tropical SST shows a stepwise decrease of 2–3 °C during this period, the East Asian monsoon gradually strengthens in response to the onset of the NHG. At the 41-kyr and 23-kyr bands, ice volume change lags tropical SST by ~4 kyr, but leads the East Asian monsoon by ~12–17 kyr. Our finding highlights the significant role of the tropical Pacific region in driving global climate change in the late Pliocene, which has invariable leading phase relative to the ice volume change as in the late Pleistocene. However, the East Asian monsoon shows a linear response to the onset of the NHG in the late Pliocene, with much bigger phase lagged at the 41-kyr and 23-kyr bands than in the Pleistocene, which suggests that at the obliquity and precession bands the phases of the Plio-Pleistocene East Asian monsoon variations relative to the global ice volume changes are not constant, but variable. Therefore, the East Asian monsoons are not only simply driven by northern summer insolation at the precession period but also modulated by global ice volume change in high latitudes.

Keywords: ODP; South China Sea; Pliocene; monsoon; tropics

1. Introduction

The first major step of global climate reorganization since the Pliocene was the onset of significant NHG ~2.75 Ma ago [1–3]. In the tropical and sub-tropical regions, this major step is reflected by periodically cooler and drier conditions in Africa after 2.8 Ma [4] and enhanced East Asian monsoonal activity between 3.6 and 2.5 Ma [5]. The geological evidence indicates some inherent relationship between the sub-tropical Asian monsoons and high northern latitude climate, as well as with tropical processes such as SST around this time [6–8]. For example, both the formation of the stony

* Corresponding author. Now at Department of Geosciences and Research Centre Ocean Margins (RCOM), Bremen University, D-28359 Bremen, Germany.
E-mail addresses: tianjun@mail.tongji.edu.cn, ian.tianjun@263.net (J. Tian).

0012-821X/$ - see front matter © 2006 Elsevier B.V. All rights reserved.
doi:10.1016/j.epsl.2006.09.028

deserts in central Australia [9] and the heightened aridity of central China correlative with Pliocene loess formation [5], show nearly synchronous bipolar sub-tropical responses to the onset of the NHG. The final closures of the Panama and Indonesian seaways, which are located in the east and west tropical Pacific, respectively, are considered to have happened 3–4 Ma ago, much earlier than significant NHG [1]. The development of the notable SST (sea surface temperature) gradient across the equatorial Pacific, which maintains the Walker circulation, occurred ~1.5–2.0 Ma ago, much later than significant NHG [3,10]. Even small changes in the tropical regions can profoundly affect the extratropical conditions, as witnessed in the interannual El Niño–Southern Oscillation phenomenon [11,12]. The records from ODP Site 806 in the western equatorial Pacific reveal that tropical SST changes lead global ice volume changes by ~3 kyr around the mid-(~0.9 Ma ago) [13] and late Pleistocene [14]. During the last two glacial–interglacial transitions, a 2–3 kyr lead of SST relative to global ice volume change is also observed in the core MD9821-62 located in the Makassar Strait in the heart of the Indo-Pacific warm pool [15]. These findings suggest that the tropical Pacific region plays an important role in driving glacial/interglacial cycles in the Pleistocene, possibly through a system similar to the El Niño–Southern Oscillation regulation of the poleward flux of heat and water vapour [15]. In contrast to tropical SST records, sub-tropical monsoonal records show a constant lag relationship of Asian monsoons with global ice volume change in the Pleistocene [6,16].

The onset of significant NHG occurred primarily between 2.5 and 3.3 Ma [17–19], although some researchers believe that the major transition happened at about 2.7 Ma based on the large-scale occurrence of ice rafted debris in the Atlantic [20]. The rapid Northern Hemisphere ice sheet expansion 2.5–3.3 Ma ago marks a transition of the Earth's climate from the permanent El Niño-like conditions during the Pliocene warm period to the amplified glacial/interglacial cycles of the ice age during the late Pliocene and Pleistocene. Unveiling the relationship of climate changes in the sub-tropical and tropical regions with the onset of the NHG will be of great help in revealing the forcing mechanism of global climate change.

2. Modern hydrology in the SCS

The modern annual mean SSS (Sea Surface Salinity) in the SCS is much lower than that in the open western Pacific by ~1.5 due to the monsoon-induced precipitation and fluvial runoff from the Eastern Asian continent and the circumjacent marginal islands [21]. The modern seasonal SSS in the southern SCS varies from 31 to 34, and the minimum SSS usually occurs during winter when the SCS is dominated by winter monsoon precipitation [22]. The precipitation radar observational data shows that the distribution of annual mean precipitation in the SCS is spatially asymmetric, with much more precipitation focused on the southern part relative to the northern (Fig. 1) [23,24]. The precipitation radar data also shows that the seasonal difference is also remarkable in the SCS, especially in the north where the summer monsoon-induced precipitation during summer dominates most of the annual precipitation [24]. However, the seasonal contrast of precipitation in the southern SCS is not as remarkable as in the north. The precipitation in the southern SCS during winter (November to January) is greater than the precipitation during summer (June to August) [24].

3. Materials and methods

We chose ODP Site 1143 in the southern SCS (9°21.72′N, 113°17.11′E, water depth 2772 m, Fig. 1), a region greatly influenced by the East Asian summer and winter monsoons, to carry out our study [25].

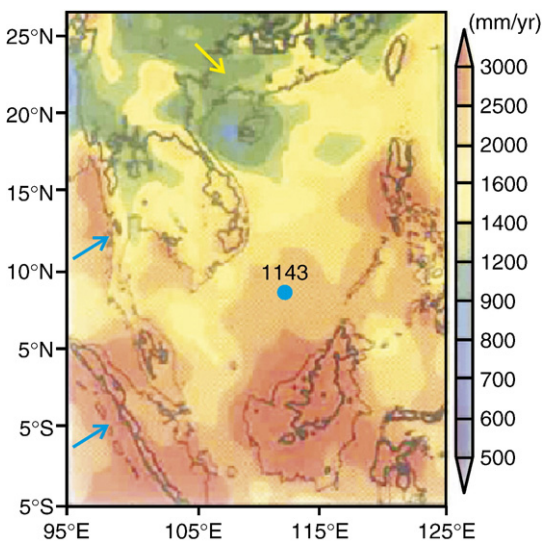

Fig. 1. Location of ODP Site 1143 in the southern South China Sea. The colors on map denote the intensity of the annual mean precipitation derived from the PR (precipitation radar) observational data [23,24]. Blue arrows denote the East Asian summer monsoon and the yellow arrow denotes the winter monsoon. (For interpretation of the references to colour in this figure legend, the reader is referred to the web version of this article.)

Site 1143 was sampled at 10 cm frequency. The preparation of samples and stable isotope analyses were performed in the State Key Laboratory of Marine Geology, Tongji University, Shanghai. Samples were soaked in tap water for 1–2 days after oven-drying at 60 °C, washed through a 63 μm sieve, oven-dried at 60 °C, then sieved to select foraminifers coarser than 150 μm for stable isotope and Mg/Ca analysis. Samples for total carbon analysis were from the same horizontal layer of the core as the stable isotope and Mg/Ca analysis.

Well preserved specimens (clean, intact, with no signs of dissolution) of the benthic foraminifers *Cibicidoides wuellerstorfi* or *Uvigerina peregrina* (when the former was not available) were selected and washed with ethanol (≥99.7%) in an ultrasonic bath at 40 kHz frequency three times for 5 to 10 seconds duration. Specimens were dried at 60 °C in an oven for 5 h, transferred to sample vials in a Finnigan automatic carbonate device (Kiel III), reacted with ortho-phosphoric acid at 70 °C to generate CO_2, then transferred to and measured in a Finnigan MAT252 mass spectrometer. Precision was regularly checked with a Chinese national carbonate standard (GBW04405) and international standard NBS19; the standard deviation was 0.07‰ for $\delta^{18}O$ during year 2000. Conversion to the international Pee Dee Belemnite (PDB) scale was performed using NBS19 and NBS18 standards. Following the standard of Shackleton and Hall [26], the $\delta^{18}O$ values of *U. peregrina* were subtracted by 0.64‰, to make them comparable to the values of *C. wuellerstorfi*.

The Mg/Ca measurements were made in the Department of Geological Sciences, University of California, Santa Barbara. Approximately 50 *G. ruber* were picked from the >150 μm fraction, gently cracked open between glass plates and divided into two equal aliquots if numbers were sufficient for replicate analyses. The fragments were transferred to microcentrifuge tubes and cleaned following a rigorous trace element cleaning process, comprised of ultrasonication and rinses for removal of clays, oxidation and reduction steps, and a final acid leach and multiple rinses in n-pure water [14,27]. Samples were analyzed on a Therm Finnigan MAT Element2 inductively coupled plasma mass spectrometer (ICP-MS) using isotope dilution [28]. Replicate analyses were performed on approximately 75% of the samples. Analytical reproducibility is estimated at 1% (1σ). Measured Mg/Ca values were converted to SST using the depth corrected Pacific *G. ruber* equation [29]. This equation considers calibrations for different species of foraminifera and quantifies the influence of dissolution by using the core depth as a correction. Tests on core top samples in different oceans suggest that *G. ruber* is the most accurate recorder of surface temperature. The bottom water of the SCS originates from the median water of the western Pacific, which insures the feasibility of this equation being used for the SST reconstruction in the SCS.

Total carbon was measured from dried and ground bulk sediment samples, and the organic carbon of carbonate free samples was measured on split samples treated with 10% HCl, washed and dried. Samples were analyzed in the State Key Laboratory of Marine Geology, Tongji University, on a Carlo Erba CHN Analyzer EA1110, of which the accuracy was 0.02% in 2005. The age model was based on tuning the benthic foraminiferal $\delta^{18}O$ to obliquity and precession [8,19], and has a good correlation to those of ODP Sites 846 and 659 [17,18]. The sedimentation rate was based on five-point Gaussian smoothing [19]. Based on the dry bulk densities [25], the sedimentation rate and the organic carbon content (wt.%), the mass accumulation rate of the TOC were calculated following Stax and Stein [30].

4. Results

4.1. Ice sheet growth in high northern latitudes

Benthic foraminiferal $\delta^{18}O$ primarily represents global ice volume change, with less than one-third of its variation connected with fluctuations of bottom water temperature and salinity, both of which have been relatively stable for the past 4 Ma [31]. The benthic foraminiferal $\delta^{18}O$ of Site 1143 over the past 5 Ma can be divided into three periods (Fig. 2a): From 5 to 3.3 Ma the late Pliocene warm period is characterized by relatively light values and stable glacial/interglacial (GI) fluctuations with small amplitudes. In the second period, the onset of significant NHG from 3.3 to 2.5 Ma is indicated by a prominent increase in $\delta^{18}O$ (Fig. 2a, c). Within this period, glacial benthic foraminiferal $\delta^{18}O$ increased from ~2.55‰ to ~3.75‰, a positive shift of ~1.2‰ within 800 kyr, whereas interglacial benthic foraminiferal $\delta^{18}O$ during interglacials only increased by ~0.6‰. The third period from 2.5 Ma to present is depicted by episodically amplified GI cycles, which were paced mainly by 41-kyr obliquity cycles prior to the Mid-Pleistocene transition (~0.9 Ma) and by 100-kyr eccentricity cycles after this transition [13]. The planktonic foraminiferal $\delta^{18}O$ of Site 1143 apparently shows a similar GI pattern before 3.3 Ma and after 2.5 Ma, with greater millennial scale variations superimposed on lower-frequency orbital scale variations (Fig. 2b). However, benthic and the planktonic foraminiferal $\delta^{18}O$ differ markedly in the second period. While the benthic foraminiferal $\delta^{18}O$ gradually increased from

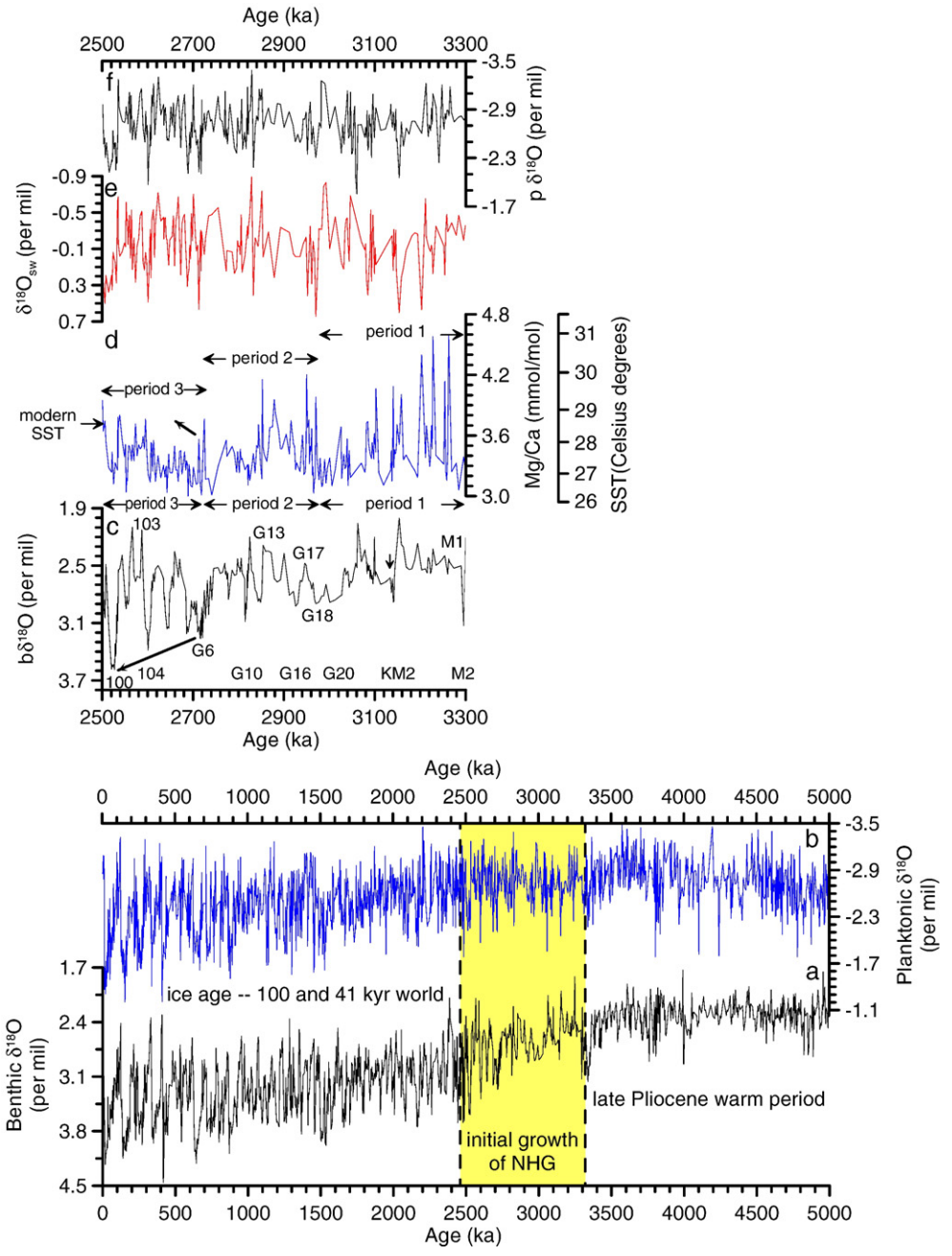

Fig. 2. Paleoceanographic time series from ODP Site 1143 marking the paleo-climate changes during the onset of the significant Northern Hemisphere Glaciation. (a), *Cibicidoides* $\delta^{18}O$ for the past 5 Ma (b), *G. ruber* $\delta^{18}O$ for the past 5 Ma. The yellow pane on (a) and (b) denotes the onset of the significant Northern Hemisphere Glaciation from 3.3 to 2.5 Ma. (c), *Cibicidoides* $\delta^{18}O$ in the period of 2.5–3.3 Ma. The letters and numbers beside the curve denote the Marine Isotope Stages (MISs). (d), *G. ruber* Mg/Ca ratio and Mg/Ca derived sea surface temperature from 3.3 to 2.5 Ma. The SST scale for Mg/Ca is exponential and is based on conversion of Mg/Ca data using the relationship: SST = ln((Mg/Ca)/0.38)/0.09 + 0.61 * 2.7 + 1.6 [29]. (e), sea water $\delta^{18}O$ calculated by using the paleotemperature equation [14]. (f), *G. ruber* $\delta^{18}O$ in the period of 2.5–3.3 Ma. (For interpretation of the references to colour in this figure legend, the reader is referred to the web version of this article.)

3.3 to 2.5 Ma (Fig. 2c), the planktonic foraminiferal $\delta^{18}O$ stayed relatively constant (Fig. 2f). In addition, while the planktonic foraminiferal $\delta^{18}O$ shows relatively invariable amplitudes of GI cycles, the benthic foraminiferal $\delta^{18}O$ shows gradually increased amplitudes of GI cycles (Fig. 2c, f).

Global ice volume, regional SST and SSS (sea surface salinity) jointly affect planktonic foraminiferal $\delta^{18}O$ [32]. Global ice volume expansion, sea surface cooling, or increase of SSS, will each result in increased planktonic foraminiferal $\delta^{18}O$. The relatively invariable planktonic foraminiferal $\delta^{18}O$, together with the gradually increased benthic foraminiferal $\delta^{18}O$ of Site 1143 2.5–3.3 Ma ago, indicates prominent local hydrological changes in the southern SCS. To initiate and sustain the significant NHG, adequate heat and moisture must be introduced from the tropics to high northern latitudes to promote accumulation of glacial ice [33]. The different behavior of the benthic and planktonic foraminiferal $\delta^{18}O$ of Site 1143 2.5–3.3 Ma ago indicates SSS changes in the western tropical Pacific coincident with ice sheet expansion.

4.2. SST changes

The *G. ruber* Mg/Ca ratio of Site 1143 varies between 3.0 and 4.6 mmol/mol, displaying clear glacial/interglacial cycles from 3.3 to 2.5 Ma (Fig. 2d).

Instrumental data from the Yongshu Reef Observatory show that the modern annual mean SST at Site 1143 is 28.6 °C, and the seasonal difference of the mean SST between summer and winter is ~2.5 °C, and the precipitation in winter is greater than in summer [34]. The reconstructed SST of ODP Site 1143 varies within a range between 31 °C and 26.4 °C from 3.3 to 2.5 Ma on millennial scale, with more than half of the record cooler than 28.4 °C (Figs. 2d, 3b). In general, our Mg/Ca derived SSTs at ODP Site 1143 show a pattern of stepwise decrease, similar to that of ODP Site 806 in the open western Pacific [10], derived from *G. sacculifer* Mg/Ca. However, the higher-resolution record from the SCS (2–3 kyr at Site 1143, compared with 10 kyr from Site 806 B) reveals the detailed structure of the temperature decrease. Corresponding to the significant NHG, the SST of ODP Site 1143 gradually decreased, punctuated by two phases of rebounding warming. As with the benthic foraminiferal $\delta^{18}O$, the SST variations of ODP Site 1143 can be divided into three periods. Period 1 is from Marine Isotope Stage (MIS) M2 to G18 (~3.3–2.97 Ma). Within this period, the SSTs show several large amplitude "spikes", oscillating around 28 °C. However, the maximum value of the "spikes" gradually decreased within this period, from ~31 °C at M2 to ~27 °C at G18, dropping nearly 4 °C while the minimum value of the "spikes" remained relatively stable. These changes resulted in decreasing amplitude of the millennial scale variability, showing a cooling trend. Period 2 of the SST variations of ODP Site 1143 is from MIS G18 to G6, marked by a rebounding warming of ~2 °C up to MIS G13 and then a following cooling of 4 °C up to MIS G6. The warming and cooling phases of period 2 are also perturbed by episodes of sharp cooling and warming respectively, such as the rapid cooling at MIS G16 during the warming phase and the gradual warming at MIS G11 during the cooling phase. Most of the SST within period 2 is below the modern SST (Fig. 2d). Period 3 is marked by a gradual warming of ~1.5–2 °C from MIS G16 to 99, gradually approaching and even exceeding modern SST. In general, the SST at ODP Site 1143 had decreased for ~5 °C from 3.3 to ~2.7 Ma, and then had rebounded by a rise of ~1.5 °C until MIS 100. In addition, the amplitude of the millennial or orbital scale variability of the SST had decreased from 3.3 to 2.5 Ma.

The benthic foraminiferal $\delta^{18}O$ and SST of Site 1143 display the same periods of variations between 3.3 and 2.5 Ma (Fig. 2c), as well as similar trends of variations and timing between periods. However, differences also exist between the two records. For example, the amplitude of glacial SST cycles gradually decreased from 3.3 to 2.5 Ma, whereas that of the benthic foraminiferal $\delta^{18}O$ gradually increased, showing an opposite pattern. After MIS G6, both the glacial and interglacial SST gradually increased with relatively low amplitudes, indicating a rebounding warming in the southern SCS after the significant NHG at ~2.7 Ma. However, at the same time, the amplitude of both glacial and interglacial benthic foraminiferal $\delta^{18}O$ increased, in response to the gradually amplified northern hemisphere ice sheet.

The relatively low-resolution Mg/Ca records of ODP Site 806 show that SST in the open western equatorial Pacific remained relatively stable from 2.7 to 2.0 Ma and then began to increase until MIS 11, decoupling with the gradually amplified global ice volume [10]. On the other hand, low-resolution Mg/Ca records from ODP Site 847 show that SST in the open eastern equatorial Pacific gradually decreased after 2.7 Ma, coupled with gradually increasing benthic foraminiferal $\delta^{18}O$. The different patterns of SST variations between the eastern and western equatorial Pacific since 2.7 Ma directly result in the increase of the SST gradient across the equatorial Pacific, firstly a weak gradient and then a prominent gradient shaping at ~2.0 Ma. This seems to indicate that while global climate descended into glacial conditions after the onset of the significant NHG 2.7 Ma ago, the El Niño-like conditions of the Pliocene Warm period weakened and gradually developed into modern conditions [3,10]. Our high-resolution SST data from the SCS generally supports the low-resolution data from the open western Pacific on secular changes, and highlights the

millennial scale variability of the SSTs. However, the amplitudes of the SST oscillations of Site 1143 after 2.7 Ma are much smaller than that of Site 806B.

5. Discussion

5.1. Monsoon-induced SSS changes

The surface water $\delta^{18}O_{sw}$ of ODP Site 1143 is calculated from the paired-planktonic foraminiferal $\delta^{18}O$ and Mg-based SST using the *Orbulina* low-light paleotemperature equation [35]. The calculated $\delta^{18}O_{sw}$ show a pattern of steady glacial/interglacial cycles from 3.3 to 2.5 Ma, without any ascending or descending trend on average. Thus, it does not represent the global ice volume change, indicating a change in regional salinity (Fig. 2e).

Ocean water $\delta^{18}O$ is associated with global ice volume changes and regional water mass salinity, the latter depending on surface water evaporation and precipitation patterns [14,31,32]. Because the increased global ice volume and its gradually expanded glacial cycles from 3.3 to 2.5 Ma, as reflected by the benthic foraminiferal $\delta^{18}O$ of Site 1143, would lead to higher $\delta^{18}O_{sw}$, the regional SSS should have decreased to compensate, resulting in relatively stable $\delta^{18}O_{sw}$. Therefore, after removing the global ice volume effects from the $\delta^{18}O_{sw}$, the residuals, the $\Delta\delta^{18}O_{sw\text{-}b}$ should represent the regional SSS variations. The temperature and salinity of the bottom water of the oceans is usually relatively invariable. For example, the bottom water temperature of the southern ocean has decreased only 4 °C during the past 5 Ma, with only ~1 °C decrease during the period of 2.5–3.3 Ma. Similarly, the bottom water temperature of the open western Pacific has decreased only 0.6 °C from 3.3 to 2.5 Ma [31]. Therefore, we obtained the $\Delta\delta^{18}O_{sw\text{-}b}$ of Site 1143 by simply subtracting the benthic foraminiferal $\delta^{18}O$ from the calculated $\delta^{18}O_{sw}$. As predicted, the calculated $\Delta\delta^{18}O_{sw\text{-}b}$ shows a stepwise decrease during the period of the significant NHG 3.3–2.5 Ma ago (Fig. 3c). The major three periods of the $\Delta\delta^{18}O_{sw\text{-}b}$ are synchronous to those of the SST, with MIS G18 and G6 being the transitional time between periods (Fig. 3b, c). Even for each period, the variations of the $\Delta\delta^{18}O_{sw\text{-}b}$ are quite similar to those of the SST. Period 1 from MIS M2 to G18 shows a gradual decrease, and period 2 shows a rebounding increase and then a further decrease, and period 3 shows a stepwise increase and then a following decrease (Fig. 3c).

The $\Delta\delta^{18}O_{sw\text{-}b}$ reflects the SSS variations at ODP Site 1143, which are associated with regional changes of

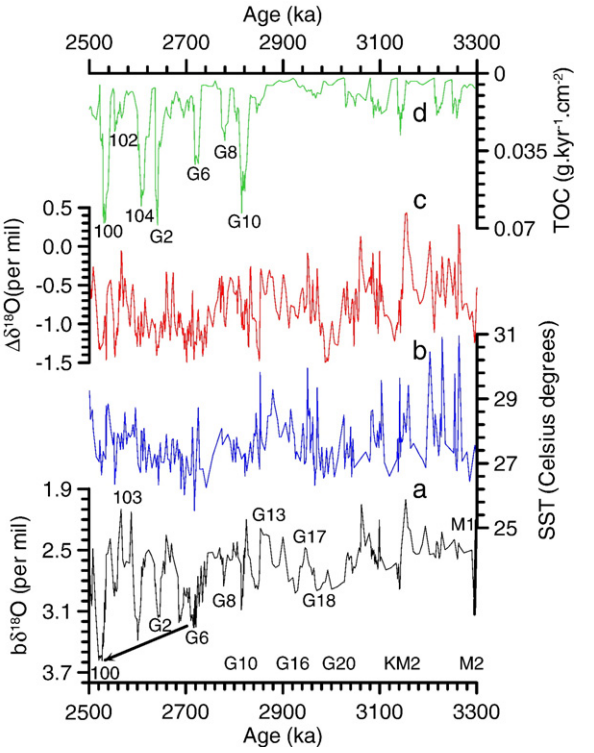

Fig. 3. Paleoceanographic time series from ODP Site 1143 in the period of 2.5–3.3 Ma. (a), *Cibicidoides* $\delta^{18}O$ in the period of 2.5–3.3 Ma. The letters and numbers beside the curve denote the Marine Isotope Stages (MISs). (b), Mg/Ca derived sea surface temperature from 3.3 to 2.5 Ma. (c), $\Delta\delta^{18}O$, the $\delta^{18}O$ difference between sea water $\delta^{18}O$ and *Cibicidoides* $\delta^{18}O$, indicating the sea surface salinity changes. (d) Total organic carbon mass accumulation rate.

precipitation and fluvial runoff. The ice sheet growth in high northern latitudes during the NHG caused an overall sea level lowering of ~43 m [36], which led to an expansion of islands such as Borneo and an extension of the southern and eastern Asian continental shelf. The extended continental shelf and islands pushed the river mouth further into the deep sea and shortened the distance between Site 1143 and the continent, leading to a decrease of SSS in the center of the basin. Analogous to modern conditions, strengthened East Asian monsoons during the NHG increased the annual mean precipitation in the southern SCS which in turn resulted in a decrease of SSS at Site 1143. Strengthened monsoons also enhanced the fluvial runoff and then further decreased SSS at Site 1143. Thus, the three periods of the $\Delta\delta^{18}O_{sw\text{-}b}$ variations from 2.5 to 3.3 Ma ago reflect a stepwise development of the East Asian monsoons during the NHG.

Modern sediment trap observations in the middle SCS lasting from 1992 to 1999 reveal that high particle fluxes usually occur during monsoon seasons, and some productivity proxies such as TOC (total organic carbon)

flux and opal flux usually reach peak values during winter [22]. In the upwelling areas of the SCS, high sea surface productivity usually occurs during monsoon seasons. However, core top studies in the SCS reveal that siliceous productivity such as opal flux is not associated with monsoon-driven upwelling, but displays a close relationship with carbonate dissolution and terrigenous dilution effects, whereas the TOC flux to a great extent shows close association with the monsoon-driven upwelling, and thus can reflect monsoon strength [24]. The down-core measurements of TOC flux at Site 1143 show clear glacial/interglacial cycles from 3.3 to 2.5 Ma, with high values during glacial periods and low values during interglacial periods. Just after 2.82 Ma (MIS G10), the amplitude of the TOC flux fluctuations within a glacial/interglacial cycle rapidly increases, reaching a level nearly 3 to 4 times the amplitude observed prior to MIS G10. We should note that the significantly larger amplitudes after 2.82 Ma are caused by greatly increased TOC flux during glacial periods and invariable TOC flux during interglacial periods. Both GCM simulations and loess/paleosol sequences reveal strong summer monsoon during interglacial periods and strong winter monsoon during glacial periods in the late Pleistocene [5,16]. Analogous to the conditions in modern and late Pleistocene periods, the variations of TOC flux of Site 1143 indicate a rapid strengthening of the East Asian winter monsoon after 2.82 Ma. Both TOC flux and $\Delta\delta^{18}O_{sw\text{-}b}$ reveal a general enhancement of the East Asian monsoons, especially the winter monsoon during the period of the late Pliocene NHG, though the two proxies differ in the timing of some larger events due to the complexity of the factors controlling proxy variations.

5.2. Orbital phase relations

It has long been speculated that insolation changes in high northern latitudes controlled by the Earth's orbital geometry dominated global climate change since at least the late Cenozoic [37,38]. This theory implies that high northern latitudes are an engine to trigger climate change, which then propagates to the mid and low latitudes through oceanic or atmospheric circulation. Therefore, climatic processes in tropical areas should lag those triggered in high northern latitude at the primary orbital periods of the eccentricity, obliquity and precession cycles. However, advances in paleoceanography in recent decades prove that tropical regions as well as atmospheric carbon dioxide play an important role in regulating global climate changes [39–41]. At least in the late Pleistocene, tropical SST change precedes the global ice volume change at both the obliquity and precession bands by ~3–4 kyr [13,14]. The glacial–interglacial transitions of tropical SST are also earlier than those of global ice volume in high northern latitudes by ~2–3 kyr, but synchronous with global increase of carbon dioxide and Antarctic warming [15]. Even in the late Pleistocene, tropical SST in the western Pacific demonstrates distinct 100-kyr, 41-kyr and 23-kyr cycles and precedes the global ice volume at these primary orbital cycles [42]. However, our late Pliocene SST records in the southern SCS are spectrally distinct from the benthic foraminiferal $\delta^{18}O$ and from the Pleistocene tropical SST records. Compared

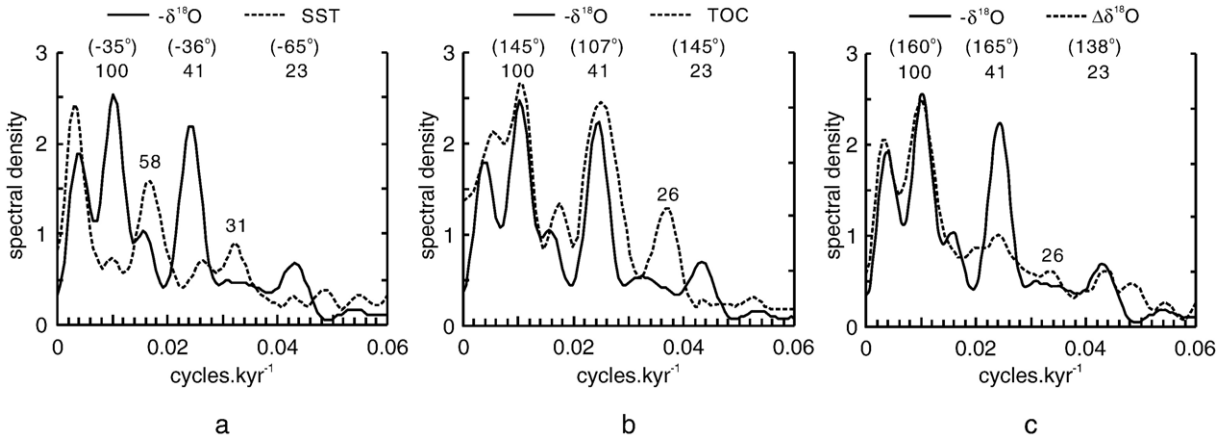

Fig. 4. Comparison among spectral analyses of *Cibicidoides* $-\delta^{18}O$ and Mg/Ca derived SST records, TOC records and $\Delta\delta^{18}O$ records from ODP Site 1143 in the period of 2.5–3.3 Ma. (a), spectrum of $-\delta^{18}O$ (solid line) and SST (dashed line). (b), spectrum of $-\delta^{18}O$ (solid line) and TOC (dashed line). (c), spectrum of $-\delta^{18}O$ (solid line) and $\Delta\delta^{18}O$ (dashed line). Numbers in the brackets of (a), (b) and (c) denote the phases at the 100-kyr, 41-kyr and 23-kyr bands. Negative phases denote SST leads $-\delta^{18}O$, and positive phases denote TOC or $\Delta\delta^{18}O$ lags $-\delta^{18}O$.

to the benthic foraminiferal $\delta^{18}O$, our SST records show weak variations at the primary orbital periodicities of 100-kyr, 41-kyr and 23-kyr, but relatively strong variations at the non-orbital periodicities of 58-kyr and 31-kyr (Fig. 4a). Coherencies at the orbital periodicities are all above the 80% alarm test level, indicating a coherent relationship between the benthic foraminiferal $\delta^{18}O$ and the SST records. Phase relations reveal a lead of the SST changes relative to the global ice volume changes at each cycle (Fig. 4a), namely a lead of 35° at the 100-kyr band, equivalent to 9.72 kyr, a lead of 36° at the 41-kyr band, equivalent to 4.1 kyr, and a lead of 65° at the 23-kyr band, equivalent to 4.1 kyr. From 3.3 to 2.5 Ma, the 3–4 kyr lead of SST change at ODP Site 1143 relative to global ice volume change at both the obliquity and precession bands is similar to that in the early Pleistocene, indicating a stationary phase relationship since the Pliocene. The consistent lead of tropical SST relative to global ice volume further indicates that the tropical Pacific region plays a momentous role in regulating global climate change at least since the late Pliocene. The highlighted 31-kyr cycle in the SST spectrum is a characterized cycle of the Pleistocene Indo-Pacific equatorial primary production and CO_2, a signature of ENSO-like control of biological production in the equatorial Indo-Pacific, indicating a significant role of the low-latitude biological pump in controlling atmospheric CO_2 concentrations [43]. The prominent 31-kyr cycle in the late Pliocene SST records at ODP Site 1143 probably suggests a CO_2 forcing of the tropical climate change. Further tests await the reconstruction of the atmospheric CO_2 in the Pliocene.

The TOC and $\Delta\delta^{18}O_{sw\text{-}b}$ are spectrally similar to the benthic foraminiferal $\delta^{18}O$, performing strong 100-kyr, 41-kyr and 23-kyr cycles (Fig. 4b). In addition, both the TOC and the $\Delta\delta^{18}O_{sw\text{-}b}$ records show a periodicity of 26 kyr which is within the range of the precession in the Pliocene [44]. The benthic foraminiferal $\delta^{18}O$ records also show a weak 26-kyr periodicity. Coherencies above the 80% alarm test level indicate coherent relationship between the benthic foraminiferal $\delta^{18}O$ and these two monsoon-related proxy records at the primary orbital periodicities. However, phase relations reveal that these two records lag the global ice volume change at the 100-kyr, 41-kyr and 23-kyr bands. The phases between the TOC and the benthic foraminiferal $\delta^{18}O$ are 145° at the 100-kyr band equating with a lag of 40.2 kyr, and 107° at the 41-kyr band equating with a lag of 12.2 kyr, and 145° at the 23-kyr band equating with a lag of 9.2 kyr (Fig. 4b). The phases between the $\Delta\delta^{18}O_{sw\text{-}b}$ and the benthic foraminiferal $\delta^{18}O$ are 160° at the 100-kyr band equating with a lag of 44.4 kyr, and 165° at the 41-kyr band equating with a lag of 18.8 kyr, and 138° at the 23-kyr band equating with a lag of 8.8 kyr (Fig. 4c). The cross-spectral analyses thus show that the global ice volume change is a factor internal to the climate system with great influence on the variability of the East Asian monsoons at least since the Pliocene. In the Pleistocene, monsoon proxy records in the SCS indicate that the monsoon maximum usually lags the minimum of the global ice volume by 2–4 kyr at both the obliquity and precession bands [6,7], much smaller than the lag of 8–18 kyr calculated in this work. The differences reveal a non-stationary phase of the East Asian monsoon relative to the global ice volume in the Plio-Pleistocene. The numerical climate-model experiment reveals that the evolution of the Asian monsoons is linked to phases of Himalaya–Tibetan plateau uplift and to the NHG. Thus, the decreased phase lag at the obliquity and precession bands is possibly linked to the amplified Northern Hemisphere ice sheets and the increased contrast between glacial and interglacial periods.

Previous studies based on low-resolution climate model hypothesize that monsoons are driven by northern summer insolation at the precession period [45]. The high-resolution dating of the late Pleistocene speleothem calcite even provides unambiguous support for this hypothesis [46,47]. The geological data from the Arabian Sea suggests that the variability in global ice volume is not a primary factor in determining the strength and timing of the monsoon winds [6]. Our geological data from the southern SCS reveals a different mechanism of the East Asian monsoon variability in the late Pliocene which shows important linkage of the East Asian monsoon with both the tropical and high latitude regions.

6. Conclusions

Our records geochemical of ODP Site 1143 from the southern SCS reveal that the East Asian monsoons gradually strengthened in response to the phased expansion of the ice sheet in the high northern latitudes during the late Pliocene, with increased phases at the obliquity and precession bands relative to the late Pleistocene. This finding suggests that the East Asian monsoons are not only simply driven by northern summer insolation at the precession period but also modulated by global ice volume change in high latitudes. The secular changes of SST in the tropical SCS show nearly synchronous stages to the significant NHG 3.3–2.5 Ma ago, but the millennial or the orbital scale variability of SST displays a totally different pattern and even leads the global ice volume change at the obliquity and precession bands. Our finding highlights the significant role of the tropical Pacific region in driving global climate change in the late Pliocene. The key factor

which affects the tele-connection of climate between low and high northern latitudes is probably the change of the concentration of CO_2 [13,48]. To prove this, the new reconstruction of CO_2 concentration in the late Pliocene will be needed.

Acknowledgements

This research used samples provided by the Ocean Drilling Program (ODP). ODP is sponsored by the U.S. National Science Foundation (NSF) and participating countries under management of Joint Oceanographic Institutions (JOI), Inc. Funding for this research was provided by the NSFC (Grant No. 40476027, 40306011, Grant No. 4999560 and Grant No. 40321603, 40331002), NKBRSF (Grant No. G2000078500). This research was also sponsored by Shanghai Rising-Star Program (A type, Grant No. 06QA14052) and the Alexander Von Humboldt Foundation. We also thank two anonymous reviewers for their constructive comments.

Appendix A. Supplementary data

Supplementary data associated with this article can be found, in the online version, at doi:10.1016/j.epsl.2006.09.028

References

[1] G.H. Haug, R. Tiedemann, Effect of the formation of the Isthmus of Panama on Atlantic Ocean thermohaline circulation, Nature 393 (1998) 673–676.
[2] G.H. Haug, D.M. Sigman, R. Tiedemann, T.F. Pedersen, M. Sarnthein, Onset of permanent stratification in the subarctic Pacific Ocean, Nature 401 (1999) 779–782.
[3] A.C. Ravelo, D.H. Andreasen, M. Lyle, A. Olivarez Lyle, M.W. Wara, Regional climate shifts caused by gradual cooling in the Pliocene epoch, Nature 429 (2004) 263–267.
[4] P.B. DeMenocal, Plio-Pleistocene African climate, Science 270 (1995) 53–59.
[5] Z.S. An, J.E. Kutzbach, W.L. Prell, S.C. Porter, Evolution of Asian monsoons and phased uplift of the Himalaya–Tibetan plateau since Late Miocene times, Nature 411 (2001) 62–66.
[6] S.C. Clemens, W. Prell, D. Murray, G. Shimmield, G. Weedon, Forcing mechanisms of the Indian Ocean monsoon, Nature 353 (1991) 720–725.
[7] S.C. Clemens, D.W. Murray, W.L. Prell, Nonstationary phase of the Plio-Pleistocene Asian monsoon, Science 274 (1996) 943–948.
[8] J. Tian, P.X. Wang, X.R. Cheng, Development of the East Asian monsoon and Northern Hemisphere glaciation: oxygen isotope records from the South China Sea, Quat. Sci. Rev. 23 (2004) 2007–2016.
[9] T. Fujioka, J. Chappell, M. Honda, I. Yatsevich, K. Fifield, D. Fabel, Global cooling initiated stony deserts in central Australia 2–4 Ma, dated by cosmogenic ^{21}Ne–^{10}Be, Geology 33 (2005) 993–996.
[10] M.W. Wara, A.C. Ravelo, M.L. Delaney, Permanent El Niño-like conditions during the Pliocene warm period, Science 309 (2005) 758–761.
[11] M. Cane, A role for the tropical Pacific, Science 282 (1998) 59.
[12] M. Cane, M. Evans, Do the tropics rule, Science 290 (2000) 1107–1108.
[13] M. Medina-Elizalde, D.W. Lea, The Mid-Pleistocene transition in the Tropical Pacific, Science 310 (2005) 1009–1012.
[14] D.W. Lea, D.K. Pak, H.J. Spero, Climate impact of late quaternary equatorial Pacific sea surface temperature variations, Science 289 (2000) 1719–1724.
[15] K. Visser, R.C. Thunell, L. Stott, Magnitude and timing of temperature change in the Indo-Pacific warm pool during deglaciation, Nature 421 (2003) 152–155.
[16] Z.L. Ding, Z.W. Yu, N.W. Rutter, T.S. Liu, Towards an orbital time scale for Chinese loess deposits, Quat. Sci. Rev. 13 (1994) 39–70.
[17] R. Tiedemann, M. Sarnthein, N.J. Shackleton, Astronomic time-scale for the Pliocene Atlantic $\delta^{18}O$ and dust flux records from Ocean Drilling Program Site 659, Paleoceanography 9 (1994) 619–638.
[18] N.J. Shackleton, S. Crowhurst, T. Hagelberg, N.G. Pisias, D.A. Schneider, A new Late Neogene time scale: application to Leg 138 Sites, Proc. Ocean Drill. Prog. Sci. Results 138 (1995) 73–101.
[19] J. Tian, P.X. Wang, X.R. Cheng, Q.Y. Li, Astronomically tuned Plio-Pleistocene benthic $\delta^{18}O$ record from South China Sea and Atlantic–Pacific comparison, Earth Planet. Sci. Lett. 203 (2002) 1015–1029.
[20] N.J. Shackleton, J. Backman, H. Zimmerman, D.V. Kent, M.A. Hall, D.G. Roberts, D. Schnitker, J.G. Baldauf, A. Desprairies, R. Homrighausen, P. Huddlestun, J.B. Keene, A.J. Kaltenback, K.A.O. Krumsiek, K.C. Morton, J.W. Murray, J. Westberg-Smith, Oxygen isotope calibration of the onset of ice-rafting and history of glaciation in the North Atlantic region, Nature 307 (1984) 620–623.
[21] S. Levitus, R. Burgett, T.P. Boyer, World Ocean Atlas, Salinity, vol. 3, US Department of Commerce, Washington DC, 1994, p. 99.
[22] J. Tian, P.X. Wang, R. Chen, X.R. Cheng, Quaternary upper ocean thermal gradient variations in the South China Sea: implications for east Asian monsoon climate, Paleoceanography 20 (2005) PA4007, doi:10.1029/2004PA001115.
[23] J. Simpson, R.F. Adler, G.R. North, A proposed tropical rainfall measuring mission, Bull. Am. Meteorol. Soc. 69 (1988) 278–295.
[24] J. Chen, P. Shi, D. Wang, Y. Du, Spatial distribution and seasonal variability of the rainfall observed from TRMM precipitation radar (PR) in the South China Sea area (SCSA), Adv. Earth Sci. 20 (2005) 29–35.
[25] P. Wang, W.L. Prell, P. Blum, Proceedings of the Ocean Drilling Program, Initial Reports, vol. 184, Ocean Drilling Program College Station, TX, 2000.
[26] N.J. Shackleton, M.A. Hall, Stable isotope record of the hole 504 sediments: high resolution record of the Pleistocene, in: J.R. Can, M.G. Langseth, et al., (Eds.), DSDP Init. Repts., vol. 69, 1983, pp. 431–441.
[27] P.A. Martin, D.W. Lea, A simple evaluation of cleaning procedures on fossil benthic foraminiferal Mg/Ca, Geochem. Geophys. Geosyst. 3 (10) (2002) 8401, doi:10.1029/2001GC000280.
[28] D.W. Lea, D.K. Pak, L.P. Peterson, K.A. Hughen, Synchroneity of tropical and high-latitude Atlantic temperatures over the last glacial termination, Science 301 (2003) 1361–1364.
[29] P.S. Dekens, D.W. Lea, D.K. Pak, H.J. Spero, Core top calibration of Mg/Ca in tropical foraminifera: refining paleo-temperature estimation, Geochem. Geophys. Geosyst. 3 (4) (2002), doi:10.1029/2001GC000200.

[30] R. Stax, R. Stein, Long-term changes in the accumulation of organic carbon in Neogene sediments, Ontong Java Plateau, Proc. Ocean Drill. Program Sci. Results 130 (1993) 573–579.
[31] C.H. Lear, Y. Rosenthal, H.K. Coxall, P.A. Wilson, Late Eocene to early Miocene ice sheet dynamics and the global carbon cycle, Paleoceanography 19 (2004) A4015, doi:10.1029/2004PA001039.
[32] N.J. Shackleton, Attainment of isotopic equilibrium between ocean water and the benthonic foraminifera genus *Uvigerina*: isotopic changes in the ocean during the last glacial, Colloq. Int. Cent. Natl. Rech. Sci. 219 (1974) 203–209.
[33] G.H. Haug, A. Ganopolski, D.M. Sigman, A. Rosell-Mele, G.E. A. Swann, R. Tiedemann, S.L. Jaccard, J. Bollmann, M.A. Maslin, M.J. Leng, G. Eglinton, North Pacific seasonality and the glaciation of North America 2.7 million years ago, Nature 433 (2005) 821–825.
[34] K.F. Yu, J.X. Zhao, K.D. Collerson, Q. Shi, T.G. Chen, P.X. Wang, T.S. Liu, Storm cycles in the last millennium recorded in Yongshu Reef, southern South China Sea, Palaeogeogr. Palaeoclimatol. Palaeoecol. 210 (2004) 89–100.
[35] B. Bemis, H. Spero, J. Bijma, D. Lea, Reevaluation of the oxygen isotopic composition of planktonic foraminifera: experimental results and revised paleotemperature equations, Paleoceanography 13 (2) (1998) 150–160.
[36] M. Mudelsee, M.E. Raymo, Slow dynamics of the Northern Hemisphere glaciation, Paleoceanography 20 (2005) PA4022, doi:10.1029/2005PA001153.
[37] M. Milankovitch, Mathematische Klimalehre und astronomishe Theorie der Klimasch-wankungen, in: W. Koppen, R. Geiger (Eds.), Handbuch der Klimatologie, vol. I(A), Gebruder Borntraeger, Berlin, 1930, pp. 1–76.
[38] A. Berger, M.F. Loutre, Insolation values for the climate of the last 10 million years, Quat. Sci. Rev. 10 (1991) 297–317.
[39] J.R. Petit, J. Jouzel, D. Raynaud, N.I. Barkov, J.M. Barnola, I. Basile, M. Bender, J. Chappellaz, M. Davisk, G. Delaygue, M. Delmotte, V.M. Kotlyakov, M. Legrand, V.Y. Lipenkov, C. Lorius, L. Pépin, C. Ritz, E. Saltzmank, M. Stievenard, Climate and atmospheric history of the past 420,000 years from the Vostok ice core, Antarctica, Nature 399 (1999) 429–436.
[40] EPICA community members, Eight glacial cycles from an Antarctic ice core, Nature 429 (2004) 623–628.
[41] U. Siegenthaler, T.F. Stocker, E. Monnin, D. Lüthi, J. Schwander, B. Stauffer, D. Raynaud, J.M Barnola, H. Fischer, V. Masson-Delmotte, J. Jouzel, Stable carbon cycle–climate relationship during the late Pleistocene, Science 310 (2005) 1313–1317.
[42] T.D. Garidel-Thoron, Y. Rosenthal, F. Bassinot, L. Beaufort, Stable sea surface temperatures in the western Pacific warm pool over the past 1.75 million years, Nature 433 (2005) 294–298.
[43] L. Beaufort, T.D. Garidel-Thoron, A.C. Mix, N.G. Pisias, Enso-like forcing on oceanic primary production during the late Pleistocene, Science 293 (2001) 2440–2444.
[44] A. Berger, M.F. Loutre, J. Laskar, Stability of the astronomical frequencies over the Earth's history for paleoclimate studies, Science 255 (1992) 560–566.
[45] J.E. Kutzbach, Monsoon climate of the early Holocene: climate experiment with Earth's orbital parameters for 9000 years ago, Science 214 (1981) 59–61.
[46] D. Yuan, C. Hai, R.L. Edwards, C.A. Dykoski, M.J. Kelly, M. Zhang, J. Qing, Y. Lin, Y. Wang, J. Wu, J.A. Dorale, Z. An, Y. Cai, Timing, duration, and transitions of the last interglacial Asian monsoon, Science 304 (2004) 575–578.
[47] W.F. Ruddiman, What is the timing of orbital-scale monsoon changes? Quat. Sci. Rev. 25 (2006) 657–658.
[48] N.J. Shackleton, The 100,000-year ice-age cycle identified and found to lag temperature, carbon dioxide, and orbital eccentricity, Science 289 (2000) 1897–1902.